Chemical retention during dry growth riming

A. L. Stuart

Department of Atmospheric Sciences, Texas A&M University, College Station, Texas, USA

M. Z. Jacobson

Department of Civil and Environmental Engineering, Stanford University, Stanford, California, USA

[1] Partitioning of volatile chemicals among the gas, liquid, and solid phases during the conversion of liquid water to ice in clouds can impact distributions of chemicals in precipitation and in the poststorm troposphere. In this paper, we extend a theoretical scaling model of chemical retention during hydrometeor freezing to all dry growth riming conditions. We account for spreading of drops upon impact with an ice-phase hydrometeor using the spread height as the mass and heat transfer length scale. To account for heat loss to the ice substrate, we use an iterative solution to calculate the total freezing time. Using this augmented development, we calculate a theoretical dimensionless retention indicator λ under the conditions of several experimental studies and compare the retention indicator to the measured retention fraction Γ. Experimental retention compares well with the retention indicator. Empirically fitting the retention indicator to the experimental data provides the first parameterization for the retention coefficient, $\Gamma = 1 - \exp(-0.002\lambda)$, that is applicable to a range of chemicals and dry growth riming conditions. The analysis and model presented in this paper can be used to improve experimental design and parameterization of retention in cloud models.   *INDEX TERMS:* 0320 Atmospheric Composition and Structure: Cloud physics and chemistry; 0365 Atmospheric Composition and Structure: Troposphere—composition and chemistry; 0368 Atmospheric Composition and Structure: Troposphere—constituent transport and chemistry; *KEYWORDS:* gas scavenging, ice chemistry, chemical partitioning

1. Introduction

[2] Convective cloud systems have many impacts on the atmosphere and climate. Through scavenging of chemical species, they contribute to acid deposition and transboundary air pollution [*Hales and Dana*, 1979]. Convective cloud systems transport and mix chemicals between the atmospheric boundary layer and upper troposphere [e.g., *Dickerson et al.*, 1987; *Chatfield and Crutzen*, 1984]. They therefore impact urban pollutant dispersal and the distributions of trace chemicals in the upper troposphere, affecting radiative fields [*Park et al.*, 2001]. They are an important source of NO_x through lightning, a key component of the global nitrogen budget [e.g., *Logan*, 1983]. Convective clouds impact upper tropospheric concentrations of ozone, which feed back to global chemical cycles and global warming [e.g., *Pickering et al.*, 1992]. They also affect the odd hydrogen budget of the upper troposphere through transport of OH precursors, such as hydrogen peroxide, acetone, formaldehyde, and other peroxides [*Prather and Jacob*, 1997; *Jaegle et al.*, 1997]. As the main oxidizing agent in the troposphere, OH in turn regulates the decomposition of nearly all atmospheric chemicals.

[3] Interactions between trace chemicals and the ice phase in clouds are not well understood despite the presence of ice in many cloud systems. In this paper, we focus on developing an understanding of chemical phase partitioning during freezing of liquid hydrometeors under dry growth riming conditions. Riming is the collision of supercooled water with ice and subsequent freezing to form graupel and hail. Dry growth riming is characterized by complete freezing of the collected drops and surface temperatures of the riming ice hydrometeor (hereafter referred to as the "rime collector") less than 0°C. In contrast, wet growth riming results in a partially frozen hydrometeor with surface temperature of 0°C.

[4] Chemical solutes originally dissolved in a supercooled water drop may be retained or expelled from the drop as it freezes on the rime collector. The degree of retention affects a chemical's availability for gas- and aqueous-phase chemical reactions and its movement in the cloud. Cloud-modeling studies that have examined the effects of chemical retention during riming have found that it may significantly impact a chemical's distribution in the troposphere and deposition to the ground [*Barth et al.*, 2001; *Audiffren et al.*, 1999; *Wang and Chang*, 1993; *Chen and Lamb*, 1990; *Cho et al.*, 1989]. Quantifying retention is important for understanding its effects on acid deposition and tropospheric chemistry.

[5] During freezing of aqueous solutions, solutes are retained to differing degrees depending on their properties and the conditions of freezing. Nonvolatile species, such as sulfate, are retained efficiently during freezing [e.g., *Borys et al.*, 1982; *Mitchell and Lamb*, 1989]. The degree of retention of more volatile species is not well characterized. Several laboratory and field studies have measured retention fractions for several gases found in clouds, including $H_2O_2, SO_2, O_2, HCl, NH_3, HNO_3, HCOOH$, and CH_3OOH [e.g., *Lamb and Blumenstein*, 1987; *Iribarne and Pyshnov*, 1990; *Snider et al.*, 1992; *Voisin et al.*, 2000]. The retention fraction Γ is the ratio of solute mass in the hydrometeor after freezing to that originally dissolved in the droplet. Measured retention fractions range from about 0.01 to 1. The reasons for the differing values are not well understood.

[6] Parameterizations of retention in cloud-modeling studies are very rudimentary. Many studies have assumed values of zeros (complete loss to the gas phase) or one (complete retention in the ice phase) [e.g., *Rutledge et al.*, 1986; *Cho et al.*, 1989; *Wang and Chang*, 1993]. Slightly more detailed parameterizations [e.g., *Mari et al.*, 2000; *Audiffren et al.*, 1999] include constant chemical-specific retention fractions for some chemicals, each based on a single experimental study. A few studies [e.g., *Kreidenweis et al.*, 1997; *Chen and Lamb*, 1994] have included a temperature-dependent expression for the SO_2 retention fraction, $\Gamma = 0.012 + 0.0058\Delta T$ (where ΔT is the difference between the supercooled drop temperature and the equilibrium freezing temperature of water), based on the experimental study of *Lamb and Blumenstein* [1987]. None of these parameterizations is consistent with the range of experimental data on retention or broadly applicable to a range of chemicals or freezing conditions in clouds.

[7] To be used with confidence in cloud modeling, a robust parameterization of retention, applicable to a broad range of chemicals and conditions, is needed. In a previous paper [*Stuart and Jacobson*, 2003] we examined the underlying drop-scale physical and chemical processes in order to develop such a parameterization. Using a scaling methodology, we proposed a theoretical dimensionless retention indicator for examining the dependence of retention on freezing conditions and chemical properties. We applied this method to investigate retention of solutes during nonrime freezing (due to contact or embedded ice nucleation) of supercooled drops in clouds and rime-freezing under conditions where spreading of drop water on impact with the rime collector is minimal. In this work, we extend the scaling model to account for spreading of drops upon impact and heat loss to the rime collector, which are important for many dry growth riming conditions. We quantitatively compare the theoretical retention indicator with available experimental data on retention during riming and develop a parameterization for the retention fraction. The resulting parameterization is generally applicable to all conditions of dry growth riming on a graupel, hailstone, or other collector.

2. Scaling Development Applied to Dry Growth Riming

[8] *Stuart and Jacobson* [2003] proposed a dimensionless number, $\lambda = \tau_{exp}/\tau_{frz}$, the ratio of the chemical expulsion time to the drop freezing time, as an indicator of retention. Here, τ_{exp} is the expulsion timescale, or the inverse rate of (one-way) chemical mass transfer from the drop. It is a function of chemical properties (including effective Henry's law constant, accommodation coefficient, and diffusivities in water and air), the drop radius, and flow in and around the drop (characterized by the drop velocity in air and properties of air and water). The term τ_{frz} is the estimated freezing time relevant to chemical retention. We consider both the total freezing time (the time for complete freezing of the drop) and the adiabatic freezing time (the time for the drop to heat to approximately 0°C). We use the adiabatic freezing time as an estimate of the time for formation of an ice shell on the surface of the drop [*Macklin and Payne*, 1967]. The retention indicator was developed from the assumption that volatile solute transfer from drops is substantially limited by ice formation. If the rate of freezing is much greater than the rate of solute transfer from the drop ($\lambda \gg 1$), we expect retention to be complete; if the rate of transfer is much greater than the rate of freezing ($\lambda \ll 1$), we expect solute loss to be complete. For λ on the order of 1, we expect λ to be directly related to retention.

[9] In our previous paper, we applied this indicator to conditions of nonrime freezing and dry growth riming when droplet spreading on impact with the rime collector is minimal. However, under many conditions of dry growth riming, drops spread significantly on impact. Drop spreading decreases the liquid layer width and, hence, increases the rate of chemical mass transfer from the drop. Drop spreading also increases the surface area for heat transfer to the underlying rime collector and, hence, increases the rate of freezing. Since chemical retention during freezing is likely a function of the relative rates of freezing and chemical expulsion from the freezing liquid, spreading (and consequent heat loss to the rime collector) may significantly impact the retention fraction. To be broadly applicable to all dry growth riming conditions, we have extended the development to include spreading, heat loss to the rime collector, and convective enhancements to energy and vapor transfer specific to riming.

2.1. Drop Spreading on Impact

[10] Spreading of drops upon impact with a rime collector under dry growth conditions has been studied experimentally and theoretically [*Brownscombe and Hallett*, 1967; *Macklin and Payne*, 1967, 1969]. During dry growth riming, drops spread on impact to a greater degree with increasing rime collector temperature and drop impact speed. Spreading is also a weak function of supercooled drop temperature and drop radius. Macklin and Payne developed the concept of a spreading factor S as the ratio of the radius after spreading to the initial drop radius. They presented experimental data on spreading under a variety of temperatures, impact speeds, and drop radii in terms of S. They also developed a simple equation for the average height of a spread cylinder on the surface of a rime collector, with equivalent volume to the original drop, as

$$h = \frac{4a}{3S^2}, \tag{1}$$

where a is the original supercooled drop radius.

[11] To account for spreading in the scaling analysis, we determine h and use it as the length scale, instead of supercooled drop radius, in the calculation of expulsion and adiabatic freezing timescales. The timescale expressions are presented and discussed by *Stuart and Jacobson* [2003]. To determine S, we interpolated and extrapolated the data presented by *Macklin and Payne* [1967], for which S is dependent on rime collector temperature, drop impact speed, and drop radius.

2.2. Heat Transfer to the Rime Collector

[12] Since there is no closed solution for the freezing time τ_{frz} that accounts for both heat loss to air and heat loss to the rime collector, we use an iterative model [after *Baker et al.*, 1987]. To solve for the freezing time, the model balances the total latent heat released due to drop freezing q_{frz} with the heat loss during the freezing time to both air q_{out} and the rime collector q_{in}, according to the following expression:

$$q_{frz} - q_{out} - q_{in} = \epsilon, \tag{2}$$

where ϵ is the convergence tolerance. The total latent heat the liquid drop releases during freezing is [e.g., *Pruppacher and Klett*, 1997]

$$q_{frz} = \frac{4}{3}\pi a^3 \rho_w [L_m - c_w(T_o - T_a)], \tag{3}$$

where ρ_w is the density of water, L_m is the latent heat of melting of water, c_w is the heat capacity of water, T_o is the equilibrium freezing temperature of water, and T_a is the air temperature. The total heat loss to the collector through the spread cylinder surface area $\pi (Sa)^2$ during any time t is determined using an expression for linear heat flow into a semi-infinite body having a plane surface [*Carslaw and Jaeger*, 1959; *Macklin and Payne*, 1967; *Baker et al.*, 1987]. This results in

$$q_{in} = 2(Sa)^2 (k_i \rho_i c_i \pi t)^{0.5}(T_o - T_s), \tag{4}$$

where a is the original supercooled drop radius, k_i is the thermal conductivity of ice, ρ_i is the density of ice, c_i is the heat capacity of ice, and T_s is the temperature of the ice substrate. However, for small enough substrates this expression is not appropriate, since it does not account for heating of the substrate. For a spherical collector, the total heat absorption capacity of the substrate (without melting) can be calculated as

$$q_c = \frac{4}{3}\pi a_i^3 \rho_i c_i (T_o - T_s), \tag{5}$$

where a_i is the rime collector radius. The heat loss to the substrate is calculated as the minimum of q_{in} and q_c. The rate of heat loss to air and total heat loss to air from a hemispherical freezing drop during any time, t, are determined from the following expressions:

$$\dot{q}_{out} = \pi a \left[Nuk_a(T_o - T_a) + ShL_vD_v\left(2\rho_w^{sat}|_{T_o} - \rho_a|_{T_a} - \rho_i^{sat}|_{T_s}\right)\right], \tag{6}$$

$$q_{out} = \dot{q}_{out}t, \tag{7}$$

respectively, where k_a is the thermal conductivity of air, L_v is the latent heat of water vaporization, D_v is the diffusivity of water vapor in air, Nu is the Nusselt number that accounts for convective enhancement to heat transfer in air, Sh is the Sherwood number that accounts for convective enhancement to water vapor mass transport in air, ρ_w^{sat} is the saturation vapor density over liquid water, ρ_i^{sat} is the saturation vapor density over ice, and ρ_a, is the water vapor density in air. Equation (6) was derived for a hemispherical drop (with the same radius as the original drop) and accounts for ventilation-enhanced conductive and evaporative transfer, after *Macklin and Payne* [1967] and *Pruppacher and Klett* [1997], respectively.

[13] To initiate the iterative model (i.e., set t in equations (4) and (7)), drop freezing times that account for only heat loss to the substrate and to air, individually, are first estimated. The initial time is calculated as the minimum of the two values. If only heat loss to air is considered, an equation for the total drop freezing time can be derived by taking the ratio of the total latent heat released q_{frz} to the rate of heat loss to air $\dot{q}_{out}$, giving

$$\tau_{f-a} = \frac{4a^2\rho_w[L_m - c_w(T_o - T_a)]}{3\left[Nuk_a(T_o - T_a) + ShL_vD_v\left(2\rho_w^{sat}|_{T_o} - \rho_a|_{T_a} - \rho_i^{sat}|_{T_s}\right)\right]}. \tag{8}$$

If only heat loss to the rime collector is important, the drop freezing time can be estimated by equating the heat loss to the substrate (equation (4)) with the total latent heat released (equation (3)) and solving for t. Using the definition of h (equation (1)), this results in the following expression [*Carslaw and Jaeger*, 1959; *Macklin and Payne*, 1967; *Baker et al.*, 1987]:

$$\tau_{f-s} = \frac{\pi\rho_w^2 h^2 [L_m - c_w(T_o - T_a)]^2}{4\rho_i c_i k_i (T_o - T_s)^2}. \tag{9}$$

This equation does not account for the finite capacity of the substrate to absorb heat. If the heat balance (equation (2)) is not adequate for this initial time guess, a new time is based on

$$t = (q_{frz} - q_{in})/\dot{q}_{out}. \tag{10}$$

The final total freezing time is determined by iterating equations (2), (4), (7), and (10) until the heat balance converges with $\epsilon < 1\%$ of q_{frz}.

2.3. Enhancement to Transfer Due to Fluid Flow

[14] To determine the expulsion and freezing times, it is necessary to consider transfer enhancement due to convective and turbulent motion in and around the drop. Here, we discuss the calculation of the Nusselt number for gas-phase heat transfer and the Sherwood numbers for water vapor and solute mass transport for the rime collector, which account for fluid-motion-induced enhancement to heat and mass transfer, respectively. For dry growth riming, we calculated the gas-phase Nu for heat transfer by treating the rime collector as a rough cylindrical collector. For flow over a bluff body,

$$Nu = ARe^m Pr^n, \tag{11}$$

where $m \approx 1/2$ and $n \approx 1/3$, but vary slightly with Re, Pr, and body shape [e.g., *Incropera and DeWitt*, 1996]. The coefficient, A varies more significantly with Re and body shape, between about 0.01 and 2.5. For smooth circular cylinders, $A \approx 0.5$. For $40 \le Re \le 1000$ and $1000 \le Re \le 2 \times 10^5$, m is 0.5 and 0.6, respectively; n is 0.37 under atmospheric conditions. For rime collectors, the surface roughness can affect heat transfer and hence the Nu. *Avila et al.* [2001] found that

$$Nu = Nu_s[1 + 1.41 \exp(-0.173 St)], \qquad (12)$$

where Nu_s is the smooth cylinder Nu and St is the Stokes number of the mean volume supercooled drop hitting the rime collector. St accounts for the ability of a drop to flow around the rime collector, and is defined as

$$St = \frac{2\rho_w a^2 v_d}{9\eta_a a_r}, \qquad (13)$$

where v_d is the velocity of the drop relative to the rime collector, and η_a is the dynamic viscosity of air [e.g., *Freidlander*, 1977]. Nu calculated with equation (12) provides values in the range of those that would result from the various parameterizations for graupel and hail described by *Pruppacher and Klett* [1997] and elsewhere [e.g., *Jayaratne*, 1993]. Sh for water vapor and solute mass transport to and from the rime collector are calculated in the same manner as Nu, but with Pr replaced by Sc. The aqueous-phase Sh for solute mass transport is calculated as that for nonriming drops [*Stuart*, 2002].

3. Comparison With Laboratory Data

[15] To test our theoretical development and develop an expression for the retention fraction, we calculated retention indicators for comparison with several experimental studies. Retention indicators were calculated as the ratio of the solute expulsion timescale τ_{exp} to the estimated freezing time τ_{frz} for both adiabatic and total freezing. These freezing times provide the range of times that may limit solute loss due to ice shell formation (adiabatic freezing time) and complete drop freezing (total freezing time) [*Stuart and Jacobson*, 2003]. Expressions for the solute expulsion timescale and adiabatic freezing time, provided by *Stuart and Jacobson* [2003], were used with h as the length scale accounting for spreading, as discussed in section 2.1. The total freezing time was estimated (section 2.2). Dimensionless numbers accounting for enhancements to transfer specific to riming conditions were calculated (section 2.3). For each experiment, parameters representative of the range of experimental conditions were used for calculations, as shown in Table 1.

[16] To determine heat transfer to the underlying substrate, the properties of the rime collector are needed. For experimental riming on cylindrical collectors, the density of the rime collector was assumed to be the density of the deposited rime. This was calculated using the parameterization of *Heymsfield and Pflaum* [1985]. For experimental freezing of drops on ice sheets, the density of the ice substrate was assumed to be that of pure ice. The density, heat capacity, and thermal conductivity of ice were all

calculated at $T_s = T_a$ using available temperature-dependent parameterizations given by *Pruppacher and Klett* [1997]. A sensitivity analysis on the dependence of retention on ice properties indicated that retention is somewhat sensitive to the ice collector density and relatively insensitive to the heat capacity and thermal conductivity. For ice densities in the range of $0.2-0.99$ g/cm^3, we found the greatest impact to be a 24% change in the calculated retention fraction. For reasonable heat capacities and thermal conductivities, we found the greatest impact to be less than a 4% change in the calculated retention fraction.

[17] Since our theoretical development does not apply to wet growth riming, but many of the experimental results include wet growth riming conditions, we only compared the theoretical retention indicator with experimental data for conditions that would result in dry growth riming. To determine whether wet or dry growth riming would likely occur, we calculated the Schumann-Ludlam limit critical liquid water content (W_c) and compared it with the experimental liquid water content. If the critical value exceeded the experimental value, the data were used. The Schumann-Ludlam limit critical liquid water content can be derived from a heat balance on the rime collector [after *Macklin and Payne*, 1967; *Young*, 1993] as

$$W_c = \frac{F}{2EVa_r[L_m - c_w(T_o - T_a)]}$$
$$\cdot \left[Nuk_a(T_o - T_{air}) + ShD_vL_s\left(\rho_i^{sat} - \rho_a\right)\right], \qquad (14)$$

where V is the impact speed of the drop on the rime collector. F is a shape factor of the rime collector with radius a_r, which equals π for a cylinder and 4 for a hailstone. E is the efficiency of collection, which is assumed to be one unless the collection efficiency was provided in the experimental data.

4. Results

[18] Figure 1a compares the experimental retention fraction with the calculated retention indicator. Experimental retention fractions for each data point on the graph represent a unique condition set or subset of reported values. For studies in which a significant trend with experimental conditions was observed (*Lamb and Blumenstein* [1987] and *Iribarne et al.* [1990] for the gravitational collection experiment), a few data points spanning the range of trend conditions are shown. Retention indicator values shown are the geometric mean between the calculated adiabatic and total freezing time retention indicator values.

[19] We see from the figure that measured retention is generally complete (solute mass is fully retained in the ice phase) for very high retention indicator values ($\gtrsim 10^4$) and reduces to near zero (near complete solute mass loss to the gas phase) for retention indicator values $\lesssim 10$. For intermediate values, much of the data are consistent with a trend in increasing experimental retention with increasing retention indicator.

[20] To develop an equation for the retention fraction Γ that is useful for cloud modeling, a function mapping the retention fraction to retention indicator λ is needed. We use an expression that fits the necessary criteria of mapping the domain space of the retention fraction ($0-1$) to that of the

Table 1. Assumed and Calculated Parameter Values for Each Experimental Study[a]

	Lamb and Blumenstein [1987]	Iribarne et al. [1990]			Iribarne and Pyshnov [1990]				Snider et al. [1992][c]	Snider and Huang [1998][c]
		Design 1[b]	Design 2[b]	Design 3[b]	NH_3	HNO_3	HCl	H_2O_2		
Atmospheric pressure, mbar	1013	1013	1013	1013	1013	1013	1013	1013	670	670
Air (and ice) temperature, °C	−2 to −20	−8 to −23	−8 to −23	−8 to −23	−5 to −12	−5 to −12	−5 to −12	−5 to −12	−8, −6.9	−9, −10
Cloud liquid water content, g/m^3	3	5	5	5	5	5	5	5	0.17, 0.19	0.15, 0.23
Drop radius, μm	8	29	29	29	29	29	29	29	6.5	4.3
Spreading factor	1.3–2.9	1.1–1.4	1.3–1.8	1.2–1.5	1.4–1.9	1.4–1.9	1.4–1.9	1.4–1.9	2.9, 3.0	2.3, 2.2
Height of spread cylinder, μm	1.2–6.0	20–30	12–24	17–27	10–18	10–18	10–18	10–18	1.0, 0.99	1.1, 1.2
Average diameter of riming collector, cm	1.2	NA	0.6	1.2	NA	NA	NA	NA	0.15	0.58
Bulk ice density of collector, g/cm^3	0.27–0.75	0.92	0.7–0.92	0.42–0.67	0.92	0.92	0.92	0.92	0.92	0.60, 0.57
Heat capacity of ice collector, cal/g/C	0.47–0.50	0.46–0.49	0.46–0.49	0.46–0.49	0.48–0.49	0.48–0.49	0.48–0.49	0.48–0.49	0.49	0.49
Thermal conductivity of ice collector, cal/cm/s/C	(5.4–5.8)E-3	(5.5–5.9)E-3	(5.5–5.9)E-3	(5.5–5.9)E-3	(5.5–5.6)E-3	(5.5–5.6)E-3	(5.5–5.6)E-3	(5.5–5.6)E-3	5.5E-03	5.5E-3, 5.6E-3
Collection efficiency	1	NA	1	1	NA	NA	NA	NA	0.78	1
Impact speed, cm/s	200	9.6–9.9	680	173	9.3–9.5	9.3–9.5	9.3–9.5	9.3–9.5	1650	1000
Air velocity over supercooled drop, cm/s	3.4–3.5	9.6–9.9	9.4–9.7	9.2–9.5	9.3–9.5	9.3–9.5	9.3–9.5	9.3–9.5	0.56	0.25
Air velocity over collector, cm/s	197	9.6–9.9	684.5	163	9.3–9.5	9.3–9.5	9.3–9.5	9.3–9.5	1900	1700
Drop pH (average)	4	2.6	2.9	3.0	6.3	2.9	2.9	NA	4.4, 4.5	4.4, 4.5
Henry's law constant (including dissociation), M/atm	800	31	60	82	3.9E + 09	3.2E + 10	1.4E + 13	6.9E + 05	6.9E + 05	6.9E + 05
Chemical gas-water accommodation coefficient	0.11	0.11	0.11	0.11	0.097	0.15	0.23	0.23	0.23	0.23
Chemical diffusivity in air, cm^2/s	0.1–0.11	0.1–0.11	0.1–0.11	0.1–0.11	0.15	0.10–0.11	0.12–0.13	0.12	0.18	0.18
Chemical diffusivity in water, cm^2/s	7.7E-06	7.7E-06	7.7E-06	7.7E-06	1.1E-05	7.5E-06	9.7E-06	1.1E-05	1.1E-05	1.1E-05
Chemical name	SO_2	SO_2	SO_2	SO_2	NH_3	HNO_3	HCl	H_2O_2	H_2O_2	H_2O_2

[a]Ranges are shown for those studies in which a range of values was used to determine the final result. NA, not applicable. Read (5.4−5.8)E-3 as $5.4–5.8 \times 10^{-3}$.

[b]Retention fraction for three distinct experimental designs were calculated: (1) gravitational collection of drops on a surface, (2) collection of drops projected on a rod, and (3) collection of drops falling onto rotating rods.

[c]Two distinct retention fraction values were calculated for comparison to experimental data subsets.
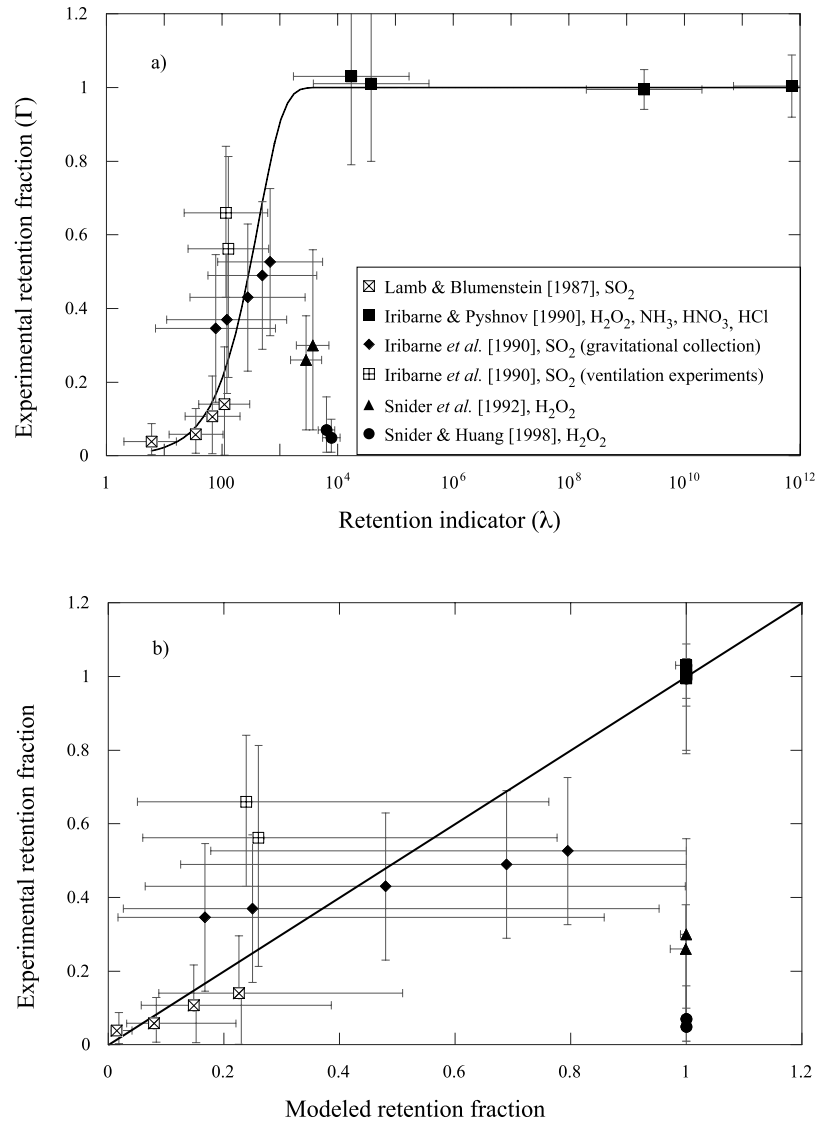
Figure 1. Experimental versus modeled retention. In Figure 1a, the independent variable is the theoretical retention indicator. The line is a curve fit for $\Gamma = 1 - \exp(-\kappa\lambda)$, giving the best fit κ of 0.002. In Figure 1b, the independent variable is the modeled retention fraction using this expression. The line is the one-to-one correspondence line. The vertical error bars indicate the range of experimental results (3 times the standard deviation for *Iribarne and Pyshnov* [1990], for which the range was not available). The horizontal range is limited by the retention indicator values for total freezing time (low values) and adiabatic freezing time (high values).

retention indicator (1×10^{-n} and 1×10^{n}, where n is a large number):

$$\Gamma = 1 - \exp(-\kappa\lambda), \tag{15}$$

where κ is a constant. To determine κ, we fit this mapping function to the data shown in Figure 1a. This results in a κ value on the order of $0.001-0.01$, with a best fit value of 0.002 (±0.001). Using the model of retention represented by equation (15) with the best fit κ, we predicted the retention fraction corresponding to each experimental data point. Figure 1b shows a comparison of modeled with measured retention fraction. The model does a reasonable job of representing the variability in measured retention values. The outlying data points are discussed in section 5.

[21] To explore the effect of spreading on retention, we performed a simple sensitivity analysis in which we set S, instead of interpolating it from experimental data. We calculated the retention indicators for each experimental study for S equal to 1 and 6. These values represent the approximate extremes of observed values. For the experimental conditions represented here, an increased spreading factor led to decreased retention indicators. This result was due to greater reductions in the expulsion time than the freezing time with increased spreading factor. The average impact on the calculated retention fraction (using equation (15) and the best fit κ) for $S = 6$ versus $S = 1$ was a decrease of 0.2.

[22] As a measure of the improvement our model provides over previous parameterizations, in Figure 2 we have
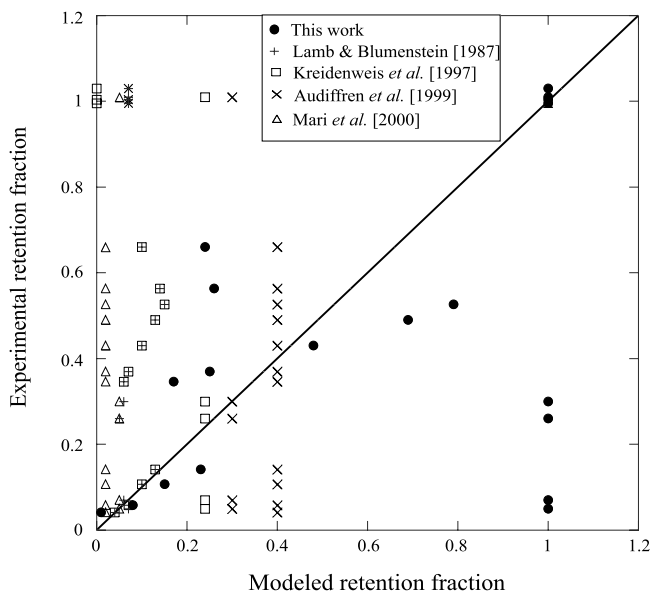
Figure 2. Comparison of retention parameterizations. Retention fraction values from each parameterization are plotted against the measured retention fraction. The *Lamb and Blumenstein* [1987] parameterization has been used in several cloud-modeling studies [e.g., *Chen and Lamb*, 1990; *Audiffren et al.*, 1999] for retention of SO_2 and other chemicals under all conditions. The *Kreidenweis et al.* [1997], *Audiffren et al.* [1999], and *Mari et al.* [2000] parameterizations are composites of distinct retention fractions for individual chemicals or groups of chemicals used for their cloud-modeling studies. For comparison, we have applied these parameterizations to all the chemicals considered here, when possible, even if they were not applied to all such chemicals in the studies. The average absolute error of modeled versus measured retention fraction for each parameterization increases in the following order: our model (0.26), Mari et al. (0.29), Audiffren et al. (0.32), Lamb and Blumenstein (0.36), and Kreidenweis et al. (0.36). The low absolute error for Mari et al. is somewhat misleading as not all experimental data points could be compared to their parameterization (data for HCl and NH_3 are therefore excluded).

compared our calculated retention fractions to those that would have resulted from applying other available parameterizations used in cloud modeling. We have excluded parameterizations that assume retention is 1 or 0 for all chemicals. The *Lamb and Blumenstein* [1987] parameterization is a curve fit from their experimental study of SO_2 retention, for which retention fraction is a function of temperature. It has been used in several cloud-modeling studies to represent retention of SO_2 [*Lamb and Chen*, 1990; *Chen and Lamb*, 1990, 1994; *Kreidenweis et al.*, 1997] and other chemicals [*Lamb and Chen*, 1990; *Audiffren et al.*, 1999]. The *Kreidenweis et al.* [1997], *Audiffren et al.* [1999], and *Mari et al.* [2000] parameterizations are composites used in their cloud-modeling studies. In each composite parameterization, distinct (constant or temperature-dependent) retention fractions are set for individual chemicals or groups of chemicals, each based on individual experimental studies. The figure indicates that

our parameterization provides the best representation of the full range of experimental data. (It also has the lowest average absolute error of modeled versus measured retention fraction.) The other parameterizations represent a few data points very well (the data upon which each was based), but poorly represent the data from other experimental studies. Our model does the best job overall, but it does not compare well to the data of *Snider et al.* [1992] and *Snider and Huang* [1998]. Possible reasons for this discrepancy are discussed in section 5. In addition, although our model can still be improved, it provides the first parameterization that explicitly represents the dependence of retention on chemical properties and riming conditions.

5. Limitations and Uncertainties

[23] Although the model provides insight into the variability within and between experimental studies, there are a few data points that do not fit well. These include the low-H_2O_2-retention results of *Snider et al.* [1992] and *Snider and Huang* [1998]. The apparent poor fit for these points may be due to (1) uncertain representation of experimental conditions and/or (2) unrepresented processes. We will discuss each of these below.

[24] The retention indicator depends on flow characteristics around freezing drops, which are a function of the riming geometry and ventilation conditions. The experimental designs differed, including riming on a flat plate, onto a steel grid, in a cone formation due to projection of drops onto a rod, and onto rotating and nonrotating cylinders. To calculate retention indicator for ventilated studies (all designs except the flat plat) we assumed a cylindrical rime collector. Its dimensions and ventilation values were based on reported data when available, or were assumed to be reasonable values. The outlying points correspond to more unusual geometries and ventilation conditions. Further, for conditions leading to significant aqueous-phase limitation to solute transfer (all studies of SO_2) the retention indicator is very dependent on the aqueous-phase ventilation coefficient. We calculated this coefficient as for non-rime freezing, since no model is available for ventilated rime collectors. This is only a crude estimate as it was developed for different conditions. The uncertain information on riming geometry and ventilation, the cylindrical rime collector assumption, and the aqueous-phase solute transfer enhancement representation may account for some of the discrepancy between outlying data points and the model.

[25] Neglect of important processes may also account for the outlying points. One process excluded from our development was chemical reaction during freezing. Aqueous-phase concentrations of SO_2 [S(IV)] and H_2O_2 are affected by reactions. During freezing, reactions may be accelerated by increased solute concentrations resulting from segregation at the ice-water interface. A few experimental studies attempted to correct for reactions. Where corrected values were available [*Lamb and Blumenstein*, 1987; *Snider et al.*, 1992; *Snider and Huang*, 1998], we used those values. However, the corrected values may not account fully for reaction effects, as only specific reactions were considered, and increased reaction rates (due to increased solute concentrations) were not considered. Reactions would likely decrease measured retention of SO_2 and H_2O_2, but would

increase that of total sulfur. The effect of reactions could be represented in the model by including a reaction timescale in the expulsion time. However, this would not account for increased reaction rates. To fully consider reactions, a numerical model at the drop scale is necessary.

[26] Our analysis also does not account for solute transfer from frozen ice during (or after) riming. J. R. Snider and coworkers [*Snider et al.*, 1992; *Snider and Huang*, 1998] theorize that retention is controlled by riming burial of frozen drops. They suggest that solute diffusion in frozen hydrometeors is faster than that generally measured for crystalline ice. Hence they suggest that the time between impaction events controls retention. Diffusivities of solutes in ice hydrometeors are not well characterized, though they have been the subject of numerous studies. Measured volume self-diffusivities of H and O in single-crystalline ice are approximately 10^{-11} cm^2/s, at $-10°$C [*Hobbs*, 1974]. Measured diffusion coefficients of other species vary widely. Diffusivities have been observed of about 10^{-12} to 10^{-11} cm^2/s for HNO$_3$ [*Sommerfeld et al.*, 1998], about 10^{-11} to 10^{-10} cm^2/s for HNO$_3$ and HCl [*Thibert and Dominé*, 1998], and about 10^{-8} cm^2/s for HNO$_3$ and HCl [*Diehl et al.*, 1995]. The greatly varying measured volume diffusivities may be due to large surface diffusivities along crystalline boundaries. *Snider and Huang* [1998] suggest that solute diffusivities in rimed ice are on the order of 10^{-8} cm^2/s, based on their riming burial theory and calculated times between droplet impacts. If solute diffusion in ice occurs at such high rates, our model does not provide a complete picture of riming retention. A dependent variable accounting for the ratio of the characteristic time for solute diffusion in ice to droplet impaction time would be needed in addition to τ_{exp}/τ_{frz}. Equilibrium (air-ice) partitioning would also have more affect on retention if diffusivities are high (retention would be less rate driven). However, current theory and data do not yet provide a convincing case for such high loss rates from ice.

[27] Finally, processes occurring at the ice-air interface may affect chemical retention. In a recent paper, *Clegg and Abbatt* [2001a] suggested that measured retention fractions of H$_2$O$_2$ and SO$_2$ may be low compared to those of strong acids (HCl, HNO$_3$) because of weaker adsorption at the ice surface. In addition, efficient reactions at the air-ice interface [e.g., *Clegg and Abbatt*, 2001b; *Conklin et al.*, 1993] have been observed. These processes are not represented here. Their impacts on retention should be considered in future studies.

6. Conclusions

[28] In this paper, we extended a scaling analysis of volatile solute retention during hydrometeor freezing to apply to all dry growth riming conditions by including drop spreading on impact, heat loss to the rime collector, and convective enhancement of energy and vapor transfer specific to riming conditions. Our analysis captures much of the variability between and within experimental studies. It provides the first semi-theoretical parameterization for chemical retention during hydrometeor freezing, $\Gamma = 1 - \exp(-0.002\lambda)$, that accounts for the variability of retention with chemical properties and freezing conditions and, hence, is applicable to a range of chemicals and dry growth

riming conditions. The development in this paper and that of *Stuart and Jacobson* [2003] indicates that the effective Henry's law constant (accounting for dissociation) is a particularly important forcing factor. According to our model, chemicals with very high effective Henry's law constants (e.g., HNO$_3$) are likely to be retained fully in the ice hydrometeor under all conditions. For chemicals with lower effective Henry's law constants (e.g., SO$_2$ and H$_2$O$_2$) pH, temperature, drop size, and air speed around the hydrometeor become important factors in the retention fraction. This suggests that cloud model parameterizations that assume all volatiles are ejected to air during freezing significantly miscalculate partitioning for highly soluble species. A better parameterization for species with high effective Henry's law constants (the cut-off being somewhere in the range of 10^6 and 10^{10} M/atm) would be to assume complete retention. For species with lower effective Henry's law constants, current parameterizations that do not account for the variability with freezing conditions (including pH, temperature, air speed, and drop size) are not robustly applicable. The inapplicability of current parameterizations is particularly important for intermediate to highly soluble species (e.g., H$_2$O$_2$ and HNO$_3$) since a recent convective cloud-modeling study [*Barth et al.*, 2001] indicates that overall cloud transport of such species (those with $K_H \gtrsim 10^5$ M/atm) may be very sensitive to the freezing retention parameterization. The work presented here indicates that future experimental studies that investigate retention should be designed to measure, control, and vary the forcing variables found in this development.

Notation

a supercooled drop radius, cm or μm.

a_r rime collector radius, cm.

c_i heat capacity of water at constant pressure, cal/g/°C.

c_w heat capacity of the ice substrate, cal/g/°C.

D_v diffusivity of water vapor in air, cm^2/s.

E rime collection efficiency.

F shape factor for the rime collector.

h mass and heat transfer length scale, cm.

K_H Henry's law constant, M/atm.

k_a thermal conductivity of air, cal/cm/s/°C.

k_a thermal conductivity of ice, cal/cm/s/°C.

L_m latent heat of water melting, cal/g.

L_s latent heat of water sublimation, cal/g.

L_v latent heat of water vaporization, cal/g.

Nu gas-phase Nusselt number (accounts for convective/turbulent enhancement to heat transfer).

Nu_s smooth cylinder Nusselt number.

Pr gas-phase Prandtl number (ratio of molecular momentum to molecular heat transfer).

q_c heat absorption capacity of the rime collector, cal.

q_{frz} total latent heat released during freezing, cal.

q_{in} total heat loss to the rime collector, cal.

q_{out} total heat loss to air, cal.

$\dot{q}_{out}$ rate of heat loss to air, cal/s.

Re Reynolds number (ratio of total to molecular momentum transfer).

S spreading factor.

Sc Schmidt number (ratio of molecular momentum to molecular mass transfer).

Sh Sherwood number (accounts for convective/turbulent enhancement to mass transfer).

St Stokes number (accounts for ability of drop to flow around rime collector).

t time guess for iterative calculation, s.

T_a air temperature, $^\circ$C.

T_o equilibrium freezing temperature of water, $^\circ$C.

T_s rime collector temperature, $^\circ$C.

V impact speed of drop on rime collector, cm/s.

v_d drop velocity relative to the rime collector, cm/s.

W_c critical liquid water content, g/cm^3.

Γ retention fraction.

ϵ error in the freezing time estimate.

η_a dynamic viscosity of air, g/cm/s.

λ retention indicator.

ρ_a water vapor density in air, g/cm^3.

ρ_i density of ice substrate, g/cm^3.

ρ_w density of the water drop, g/cm^3.

ρ_i^{sat} saturation vapor density over ice, g/cm^3.

ρ_w^{sat} saturation vapor density over liquid water, g/cm^3.

τ_{exp} overall solute expulsion timescale, s.

τ_{f-a} freezing time considering only heat loss to air, s.

τ_{f-s} freezing time considering only heat loss to the rime collector, s.

τ_{frz} total freezing time, s.

References

Audiffren, N., S. Cautenet, and N. Chaumerliac (1999), A modeling study of the influence of ice scavenging on the chemical composition of liquid-phase precipitation of a cumulonimbus cloud, *J. Appl. Meteorol.*, *38*, 1148–1160.

Avila, E. E., R. G. Pereyra, N. E. Castellano, and C. P. R. Saunders (2001), Ventilation coefficients for cylindrical collectors growing by riming as a function of the cloud droplet spectra, *Atmos. Res.*, *57*, 139–150.

Baker, B., M. B. Baker, E. R. Jayaratne, J. Latham, and C. P. R. Saunders (1987), The influence of diffusional growth rates on the charge transfer accompanying rebounding collisions between ice crystals and soft hailstones, *Q. J. R. Meteorol. Soc.*, *113*, 1193–1215.

Barth, M. C., A. L. Stuart, and W. C. Skamarock (2001), Numerical simulations of the July 10, 1996, Stratospheric-Tropospheric Experiment: Radiation, Aerosols, and Ozone (STERAO)-Deep Convection experiment storm: Redistribution of soluble tracers, *J. Geophys. Res.*, *106*(D12), 12,381–12,400.

Borys, R. D., P. J. Demott, E. E. Hindman, and D. Feng (1982), The significance of snow crystal and mountain-surface riming to the removal of atmospheric trace constituents from cold clouds, in *Precipitation Scavenging, Dry Deposition, and Resuspension: Proceedings of the Fourth International Conference*, pp. 181–189, Elsevier Sci., New York.

Brownscombe, J. L., and J. Hallett (1967), Experimental and field studies of precipitation particles formed by the freezing of supercooled water, *Q. J. R. Meteorol. Soc.*, *93*, 455–473.

Carslaw, H. S., and J. C. Jaeger (1959), *Conduction of Heat in Solids*, 510 pp., Oxford Univ. Press, New York.

Chatfield, R. B., and P. J. Crutzen (1984), Sulfur dioxide in remote oceanic air: Cloud transport of reactive precursors, *J. Geophys. Res.*, *89*(D5), 7111–7132.

Chen, J.-P., and D. Lamb (1990), The role of precipitation microphysics in the selective filtration of air entering the upper troposphere, in *1990 Conference on Cloud Physics*, pp. 479–484, Am. Meteorol. Soc., Boston, Mass.

Chen, J.-P., and D. Lamb (1994), Simulation of cloud microphysical and chemical processes using a multicomponent framework. Part I: Description of the microphysical model, *J. Atmos. Sci.*, *51*(18), 2613–2630.

Cho, H. R., M. Niewiadomski, and J. Iribarne (1989), A model of the effect of cumulus clouds on the redistribution and transformation of pollutants, *J. Geophys. Res.*, *94*(D10), 12,895–12,910.

Clegg, S. M., and J. P. D. Abbatt (2001a), Uptake of gas-phase SO$_2$ and H$_2$O$_2$ by ice surfaces: Dependence on partial pressure, temperature, and surface acidity, *J. Phys. Chem. A*, *105*, 6630–6636.

Clegg, S. M., and J. P. D. Abbatt (2001b), Oxidation of SO$_2$ by H$_2$O$_2$ on ice surfaces at 228K: A sink for SO$_2$ in ice clouds, *Atmos. Chem. Phys.*, *1*, 73–78.

Conklin, M. H., R. A. Sommerfeld, S. K. Laird, and J. E. Villinski (1993), Sulfur dioxide reactions on ice surfaces: Implications for dry deposition to snow, *Atmos. Environ., Part A*, *27*, 2927–2934.

Dickerson, R. R., et al. (1987), Thunderstorms: An important mechanism in the transport of air pollutants, *Science*, *235*, 460–465.

Diehl, K., S. K. Mitra, and H. R. Pruppacher (1995), A laboratory study of the uptake of HNO$_3$ and HCl vapor by snow crystals and ice spheres at temperatures between 0 and -40 C, *Atmos. Environ.*, *29*, 975–981.

Freidlander, S. K. (1977), *Smoke, Dust, and Haze: Fundamentals of Aerosol Behavior*, 317 pp., John Wiley, Hoboken, N. J.

Hales, J. M., and M. T. Dana (1979), Precipitation scavenging of urban pollutants by convective storm systems, *J. Appl. Meteorol.*, *18*(3), 294–316.

Heymsfield, A. J., and J. C. Pflaum (1985), A quantitative assessment of the accuracy of techniques for calculating graupel growth, *J. Atmos. Sci.*, *42*(21), 2264–2274.

Hobbs, P. V. (1974), *Ice Physics*, Clarendon, Oxford, UK.

Incropera, F. P., and D. P. DeWitt (1996), *Introduction to Heat Transfer*, John Wiley, Hoboken, N. J.

Iribarne, J. V., and T. Pyshnov (1990), The effect of freezing on the composition of supercooled droplets: I. Retention of HCl, HNO$_3$, NH$_3$, and H$_2$O$_2$, *Atmos. Environ., Part A*, *24*, 383–387.

Iribarne, J. V., T. Pyshnov, and B. Naik (1990), The effect of freezing on the composition of supercooled droplets: II. Retention of S (IV), *Atmos. Environ., Part A*, *24*, 389–398.

Jaegle, L., et al. (1997), Observed OH and HO$_2$ in the upper troposphere suggest a major source from convective injection of peroxides, *Geophys. Res. Lett.*, *24*(24), 3181–3184.

Jayaratne, E. R. (1993), The heat balance of a riming graupel pellet and the charge separation during ice-ice collisions, *J. Atmos. Sci.*, *50*(18), 3185–3193.

Kreidenweis, S. M., Y. Zhang, and G. R. Taylor (1997), The effects of clouds on aerosol and chemical species production and distribution: 2. Chemistry model description and sensitivity analysis, *J. Geophys. Res.*, *102*(D20), 23,867–23,882.

Lamb, D., and R. Blumenstein (1987), Measurement of the entrapment of sulfur dioxide by rime ice, *Atmos. Environ.*, *21*, 1765–1772.

Lamb, D., and J.-P. Chen (1990), A modeling study of the effecs of ice-phase microphysical processes on trace chemical removal efficiencies, *Atmos. Res.*, *25*, 31–51.

Logan, J. A. (1983), Nitrogen oxides in the troposphere: Global and regional budgets, *J. Geophys. Res.*, *88*, 10,785–10,807.

Macklin, W. C., and G. S. Payne (1967), A theoretical study of the ice accretion process, *Q. J. R. Meteorol. Soc.*, *93*, 195–213.

Macklin, W. C., and G. S. Payne (1969), The spreading of accreted droplets, *Q. J. R. Meteorol. Soc.*, *95*, 724–730.

Mari, C., D. J. Jacob, and P. Bechtold (2000), Transport and scavenging of soluble gases in a deep convective cloud, *J. Geophys. Res.*, *105*(D17), 22,255–22,267.

Mitchell, D. L., and D. Lamb (1989), Influence of riming on the chemical composition of snow in winter orographic storms, *J. Geophys. Res.*, *94*(D12), 14,831–14,840.

Park, R. J., G. L. Stenchikov, L. E. Pickering, R. R. Dickerson, D. J. Allen, and S. Kondragunta (2001), Regional air pollution and its radiative forcing: Studies with a single-column chemical and radiation transport model, *J. Geophys. Res.*, *106*(D22), 28,751–28,770.

Pickering, K. E., A. M. Thompson, J. R. Scala, W.-K. Tao, R. R. Dickerson, and J. Simpson (1992), Free tropospheric ozone production following entrainment of urban plumes into deep convection, *J. Geophys. Res.*, *97*(D16), 17,985–18,000.

Prather, M. J., and D. J. Jacob (1997), A persistent imbalance in HO$_x$ and NO$_x$ photochemistry of the upper troposphere driven by deep tropical convection, *Geophys. Res. Lett.*, *24*(24), 3189–3192.

Pruppacher, H. R., and J. D. Klett (1997), *Microphysics of Clouds and Precipitation*, 954 pp., Kluwer Acad., Norwell, Mass.

Rutledge, S. A., D. A. Hegg, and P. V. Hobbs (1986), A numerical model for sulfur and nitrogen scavenging in narrow cold-frontal rainbands: 1. Model description and discussion of microphysical fields, *J. Geophys. Res.*, *91*(D13), 14,385–14,402.

Snider, J. R., and J. Huang (1998), Factors influencing the retention of hydrogen peroxide and molecular oxygen in rime ice, *J. Geophys. Res.*, *103*(D1), 1405–1415.

Snider, J. R., D. C. Montague, and G. Vali (1992), Hydrogen peroxide retention in rime ice, *J. Geophys. Res.*, *97*(D7), 7569–7578.

Sommerfeld, R. A., C. A. Knight, and S. K. Laird (1998), Diffusion of HNO_3 in ice, *Geophys. Res. Lett.*, *25*(6), 935–938.

Stuart, A. L. (2002), Volatile chemical partitioning during hydrometeor freezing and its effects on tropospheric chemical distributions, Ph.D. thesis, Stanford Univ., Stanford, Calif., Aug.

Stuart, A. L., and M. Z. Jacobson (2003), A timescale investigation of volatile chemical retention during hydrometeor freezing: Nonrime freezing and dry growth riming without spreading, *J. Geophys. Res.*, *108*(D6), 4178, doi:10.1029/2001JD001408.

Thibert, E., and F Dominé (1998), Thermodynamics and kinetics of the solid solution of HNO_3 in ice, *J. Phys. Chem. B*, *102*, 4432–4439.

Voisin, D., M. Legrand, and N. Chaumerliac (2000), Scavenging of acidic gases (HCOOH, CH_3OOH, HNO_3, HCl, and SO_2) and ammonia in mixed liquid-solid water clouds at Puy de Dome mountain (France), *J. Geophys. Res.*, *105*(D5), 6817–6835.

Wang, C., and J. S. Chang (1993), A three-dimensional numerical model of cloud dynamics, microphysics, and chemistry: 3. Redistribution of pollutants, *J. Geophys. Res.*, *98*(D9), 16,787–16,789.

Young, K. C. (1993), *Microphysical Processes in Clouds*, Oxford Univ. Press, New York.

————————————

M. Z. Jacobson, Department of Civil and Environmental Engineering, Stanford University, Stanford, CA 94305-4020, USA. (jacobson@stanford.edu)

A. L. Stuart, Department of Atmospheric Sciences, Texas A&M University, College Station, TX 77843-3150, USA. (amystuart@tamu.edu)